Residual axial capacity of reinforced concrete columns with simulated blast damage

Li, Bing; Nair, Anand; Kai, Qian

2012

Li, B., Nair, A., & Kai, Q. (2012). Residual Axial Capacity of Reinforced Concrete Columns with Simulated Blast Damage. ASCE Journal of Performance of constructed facilities, 26(3), 287.

https://hdl.handle.net/10356/94134

https://doi.org/10.1061/(ASCE)CF.1943-5509.0000210

Residual Axial Capacity of Reinforced Concrete Columns with Simulated Blast Damage

Bing Li[1]; Anand Nair[2]; and Qian Kai, A.M.ASCE[3]

[1]Associate Professor, School of Civil and Environmental Engineering, Nanyang Technological Univ., Singapore 639798 (corresponding author). E-mail: cbli@ntu.edu.sg

[2]Engineer, Land Transport Authority (LTA), Singapore 408865. [3]Research Associate, School of Civil and Environmental Engineering, Nanyang Technological Univ., Singapore 639798.

Abstract: Two specimen series [limited seismic (LS) and nonseismic (NS)] were subjected to quasistatic loadings to evaluate the residual axial capacity of blast-damaged reinforced concrete (RC) columns. A validated numerical model was used to predict the residual lateral deflection of RC columns subjected to an explosive attack. Three hydraulic actuators were installed horizontally to reproduce the target residual lateral deflection as predicted through this numerical model. Another two hydraulic actuators were installed vertically to apply the axial load and measure the residual axial capacity of the damaged columns. The effects of parameters such as axial loading and the transverse reinforcement ratio are investigated through this study. The results obtained from the experimental study showed the improved performance that LS detailing provided to RC columns to resist blast or lateral loads. This subsequently led columns detailed with a higher transverse reinforcement ratio to have an increased residual axial capacity when laterally damaged, as compared with the NS detailed specimens. Axial load (service load) on the columns was also found to affect the residual deflection profile and residual axial capacity of the columns after the specified blast event. The validity range of a previously published function to determine blast-damaged residual axial capacity of RC columns is refined through the results obtained. **DOI: 10.1061/(ASCE)CF.1943-5509.0000210.**

CE Database subject headings: Concrete columns; Reinforced concrete; Finite-element method; Axial loads; Blast loads.

Author keywords: Reinforced concrete column; Residual axial capacity; Finite-element analysis; Column transverse reinforcement; Column axial load.

Introduction

Background

Terrorist attacks in the past decades have drawn attention to the deficiencies in current structural design practices. These attacks served as a call to action to reevaluate current design practices to accommodate for these severe loads where required (Li et al. 2009, 2011). Failure of an individual column element could possibly trigger a progressive collapse of the entire frame structure. Detonation of explosive devices results in the generation of highly pressurized hot gasses, which expand violently and displace the

surrounding air, causing the reinforced concrete (RC) column element to lose its capacity as it accumulates damage. The postblast residual axial capacity of an RC column is therefore narrowed down to be an important behavior to focus on. It would be extremely important to understand the damage sustained by a, RC column element and the residual axial capacity to be able to determine if a progressive collapse of the entire structure could ensue.

A series of test was conducted by Crawford et al. (2001) to quantify the effects of explosive loads on conventional buildings. The full-scale tests were conducted on RC columns that are typically found in four-storey office buildings located within Seismic Zone 1 of the East Coast of the United States. The test results indicated that the RC column element in the frame structure has a low lateral load capacity and low ductility. The explosion was set off at a short standoff distance. The loosely spaced transverse reinforcement within the RC column caused the column to fail owing to both its shear and flexure capacity to be exceeded at both ends. An additional experiment was conducted by the research team to determine the increase in blast-loading capacity of the RC column when reinforced with a layer of carbon fiber-reinforced polymer (CFRP). It was apparent from the results obtained that the retrofitted column remained elastic and sustained no permanent deformations. The improvement provided by the retrofit was evident from this study.

Crawford et al. (2001) furthered works and developed a column test fixture for conducting field tests. A series of test programs were conducted with this test setup. They involved TNT-equivalent weights varying from 500–1,000 kg that were placed at standoff distances of 3.0–6.0 m. It was observed from the results that the RC column core concrete was split into small segments by diagonal shear cracks. Crawford et al. (2001) also proceeded to carry out an experimental study in a laboratory. The aim of this experiment was to obtain detailed response data regarding the behavior of RC columns under carefully controlled conditions. The study showed that the laboratory tests were capable of producing deformation results on RC columns similar to the results achieved from the field tests.

A dynamic structure collapse experiment with a 1/4-scale building model was conducted by Krauthammer et al. (2003). A numerical study was also conducted on a model of the specimen by the research team. Finite-element (FE) analyses using a Lagrangian large deformation code with an explicit-dynamic FE computer code were able to predict the response with reasonable accuracy.

To evaluate the progressive collapse performance of the Alfred P. Murrah Federal Building, Oklahoma City, OK, which was severely damaged in a 1995 terrorist attack, a study was conducted by Hayes et al. (2005) to determine if current seismic design provisions could sufficiently improve the resistance of RC columns subjected to blast loads to possibly prevent progressive collapse of the structure. The building was initially evaluated for seismic vulnerabilities as if it were located in a high-seismicity region. Strengthening schemes in the form of a pier-spandrel system, a special moment concrete frame, and a set of internal shear walls were proposed. The strengthened structure was then analyzed for its response to the same explosion that occurred in 1995. The analysis results showed that the pier-spandrel and the special moment frame schemes reduced the degree of direct blast-induced damage and was capable of preventing progressive collapse of the building.

In a more recent parametric study conducted by Bao and Li (2010) and Wu et al. (2011), the significance of selected parameters that affected the residual axial strength of a blast-damaged RC column was revealed. Bao and Li (2010) proposed a formula that was capable of providing a term v, described as the ratio of the residual axial strength of a blast-damaged column to its initial axial capacity. This ratio is defined as follows:

$$v = \frac{(P_r - P_L)}{(P_{\max} - P_L)} \qquad (1)$$

where P_r = residual axial capacity of a blast-damaged column; P_L = axial load that the column is designed to sustain; and P_{max} = axial capacity of an undamaged column. As such, when a column is undamaged, P_r = $P_{max,}$ and the value of v = 1:0. Likewise, when the column has totally lost the ability to sustain its axial load, $P_r = P_L$, and the value of v = 0:0. This also refers to the ultimate state of the column.

The various parameters used in this study provided a means of determining this residual axial strength ratio through a multivariable regression analysis. This ratio was proposed to be determined by its authors as:

$$v = \left[73.65\rho_v + 8.47\rho_g - 0.021\left(\frac{L}{b}\right) + 0.104\right] e^{\left[89284.22\rho_v - 1308.64\rho_g - 9.68\left(\frac{L}{b}\right) - 382.12\right]\left(\frac{y_r}{L}\right)\left(\frac{P_L}{f'_c}/A_g\right)} \quad (2)$$

where ρ_v = transverse reinforcement ratio; ρ_g = longitudinal reinforcement ratio; L = height of the column; b = width; y_r = residual midheight deflection owing to the blast; P_L = axial load; $f'c$ = compressive strength of the concrete used; and A_g = gross column cross-sectional area.

Some of the findings from this study included that the effect of axial load ratio is more critical for columns with lower transverse reinforcement ratio and that the ratio of residual axial capacity increases as longitudinal reinforcement ratio was increased. The comparison made between the results from the proposed equation and the analytical results showed that the equation was capable of predicting the residual axial capacity of blast-damaged columns with reasonable accuracy.

Although existing literature on residual axial capacity of RC columns provides some numerical and experimental investigations, the effects of two critical factors, namely the effect of increased transverse reinforcement and the effect of axial loading, have not been clearly shown. Moreover, experimental studies to determine the residual capacity of RC column subjected to blast loadings are limited. Therefore, a series of experimental tests were designed to be tested in the Protective Engineering Laboratory of Nanyang Technological University, Singapore. With three horizontally mounted hydraulic actuators, the damage profile attained by the model column from the numerical simulation was recreated on actual column specimens during the experimental program. The damage profile was predicted using a validated numerical model that was capable of predicting the residual lateral deflection of RC columns subjected to blast loads.

Test Specimens

Two series of RC columns, referred to as “LS” (limited seismic detailing) and “NS” (nonseismic detailing), were constructed to be tested for this study. The variables that were selected to be studied included the spacing of transverse reinforcement within the column and axial loading. Fig. 1 shows the schematic dimensions and detailing of all the test specimens. In the LS series (specimens S1 and S3), hoop stirrups with a 135° bend were used as transverse reinforcements. The transverse reinforcement was detailed with a closer spacing as compared with the NS series. The transverse reinforcement ratio for the LS series is 0.58%. In the NS series (specimens S2 and S4), hoop stirrups with a 90° bend were used as transverse reinforcements. The transverse reinforcement ratio for the NS series is 0.19%. Both series of specimens had a cross-sectional dimension of 260 × 260 mm and a vertical height of 2,400 mm. A higher axial load of $0.4f\,'_cA_g$ was applied on the top head of the column for specimens S1 and S2, whereas for specimens S3 and S4, a lower axial load of $0.2f'_cA_g$ was prescribed. A summary of column specimen specifications is shown in Table 1.

Finite-Element Analysis to Predict Residual Lateral Deflection

General

The nonlinear FE modeling software LS-DYNA (Hallquist 2008) was used in this study to carry out the numerical analysis. LSDYNA (Hallquist 2008) is a fully integrated engineering analysis code specifically designed for nonlinear dynamic problems. It is particularly suited to the modeling of explosion events.

Blast Loadings

An exterior explosion could produce four types of loads: impact of primary fragments, impact of secondary fragments, overpressure, and reflected pressure. The effect of overpressure and reflected pressure on the target from an explosion was investigated in this study. Because the overpressure wave strikes on the front face of a closed target, a reflected pressure is instantly developed, and this is the most destructive aspect of blast loading on a structure. The loading at different points on the front surface of the column for a given charge and standoff distance is computed by LS-DYNA (Hallquist 2008) with a built-in ConWep blast model, which relates the reflected overpressure to the scaled distance and accounts for the angle of incidence of the blast wave (RandersPehrson and Bannister 1997). Blast incidents in recent years showed that most terrorist attacks on public structures were explosions within short standoff distance (< 10 m). Thus, in this study, the standoff distance is assumed to be 7.2 m. Considering the limitation of the weight of explosive, which can be obtained in any particular region, an equivalent weight of 1,000 kg of TNT was selected for this study.

Structural Geometry Modeling

The typical geometry FE models of LS and NS specimens are shown in Fig. 2. Eight-node solid hexahedron elements were used to represent concrete. The reinforcing bars are modeled explicitly using two-node Hughes-Liu beam elements. Perfect bond conditions were assumed. This implies complete compatibility of strains between concrete and steel. The restraint at the upper end of the column provided by secondary floor beams and slabs were modeled as a stiff block, whereas the bottom end restraint was modeled as a fixed support. A rigid plate, which is allowed to move in only the vertical direction, is attached to the top end of the model.

Material Modeling

Modeling of Concrete

The FE code LS-DYNA (Hallquist 2008) contains several material models that can be used to represent concrete. The material model MAT_CONCRETE_DAMAGE_REL3, available in LS-DYNA (Hallquist 2008), is used in this study to model the concrete. It is a plasticity-based model that uses three shear failure surfaces and includes damage and strain-rate effects (Malvar et al. 1997). The model has a default parameter generation function using the unconfined compressive strength of the concrete and provides a robust representation of complex concrete laboratory response (Schwer and Malvar 2005). In this model, the stress tensor is expressed as the sum of the hydrostatic stress tensor and the deviatoric stress tensor. The hydrostatic tensor changes the concrete volume, and the deviatoric stress tensor controls the shape deformation.

The compaction model for the hydrostatic stress tensor is a multilinear approximation in internal energy. Pressure is defined by

$$p = C(\varepsilon_v) + \gamma T(\varepsilon_v)E \qquad (3)$$

where E = internal energy per initial volume; and γ = ratio of specific heats. The volumetric strain ε_v is given by the natural logarithm of the relative volume and is shown in Fig. 3. The model contains an elastic path from the hydrostatic tension cutoff to the point *T* of elastic limit. When the tension stress is greater than the hydrostatic tension cutoff, tension failure occurs. When the volumetric strain exceeds the elastic limit, compaction occurs, and the concrete turns into a granular kind of material. The bulk unloading modulus is a function of volumetric strain. Unloading occurs along the unloading bulk modulus up to the pressure cutoff. Reloading always follows the unloading path to the point at which unloading began and continues along that loading path.

A three-curve model is used to analyze the deviatoric stress tensor; the upper curve represents the maximum strength curve, the middle curve is the initial yield strength curve, and the lower curve is the failed material residual strength curve.

To consider that concrete would exhibit an increased strength under higher loading rates, a dynamic increase factor (DIF), the ratio of the dynamic -to -static strength, is employed in this analysis. The expressions proposed by Malvar and Crawford (1998) are used. The DIF for the concrete compressive strength is given as

$$\mathrm{DIF} = \begin{cases} \left(\frac{\dot{\varepsilon}}{\dot{\varepsilon}_s}\right)^{1.026\alpha_s} & \dot{\varepsilon} \le 30\mathrm{s}^{-1} \\ \gamma_s \left(\frac{\dot{\varepsilon}}{\dot{\varepsilon}_s}\right)^{\frac{1}{3}} & \dot{\varepsilon} > 30\mathrm{s}^{-1} \end{cases} \qquad (4)$$

where $\dot{\varepsilon}$ = strain rate in the range of 30×10^{-6} to 300 s^{-1}; $\dot{\varepsilon}_s = 30 \times 10^{-6}\ \mathrm{s}^{-1}$ (static strain rate); $\log \gamma_s = 6.156\alpha_s - 2$; $\alpha_s = 1/(5 + 9f_c/f_{co})$; f_{co} = 10 MPa; and f_c = static compressive strength of concrete.

The DIF for concrete in tension is given by

$$\mathrm{DIF} = \begin{cases} \left(\frac{\dot{\varepsilon}}{\dot{\varepsilon}_s}\right)^{\delta} & \dot{\varepsilon} \le 1.0\ \mathrm{s}^{-1} \\ \beta\left(\frac{\dot{\varepsilon}}{\dot{\varepsilon}_s}\right)^{\frac{1}{3}} & \dot{\varepsilon} > 1.0\ \mathrm{s}^{-1} \end{cases} \qquad (5)$$

where ε = strain rate in the range of $10^{-6}\ \mathrm{s}^{-1}$ to $160\ \mathrm{s}^{-1}$; $\dot{\varepsilon}_s = 10^{-6}\ \mathrm{s}^{-1}$ (static strain rate); $\log \beta = 6\delta - 2\delta = 1/(1 + 8f_c/f_{co})$; f_{co} = 10 MPa; and f_c = static compressive strength of concrete. Different rate enhancements are specified for "tension and compression" in the concrete material model employed in this study owing to the tensile response being more sensitive to strain rate in contrast to the compressive response.

The strain-rate effect in the numerical model is incorporated at any given pressure by expanding the failure surfaces with a rate enhancement factor in accordance to the effective deviatoric strain rate. Defining the strain-rate enhancement factor as r_f and the pressure as p, an "unenhanced" pressure p / r_f is first obtained. Then the unenhanced strength $\Delta\sigma(p / r_f)$ is calculated for the specified failure surface. Finally, the enhanced strength is obtained by

$$\Delta\sigma_e = r_f \Delta\sigma \left(\frac{p}{r_f}\right) \qquad (6)$$

Strength is equally enhanced along any radial stress path that includes uniaxial, biaxial, and triaxial tension and uniaxial and biaxial compression. The effective strain rate versus deviatoric strength enhancement is given by an LS-DYNA DEFINE_CURVE keyword.

Modeling of Reinforcement

The material model MAT_PLASTIC_KINEMATIC is used to model the steel. It is an elastic-plastic material model with strain-rate effect. The stress-strain curve is assumed bilinear, to represent the elastoplastic behavior with linear isotropic hardening. The expressions proposed by Malvar and Crawford (1998) are used to incorporate for strain-rate sensitivity. The adopted DIF formulation was for both yield and ultimate stress

$$\text{DIF} = \left(\frac{\dot{\varepsilon}}{10^{-4}}\right)^{\alpha} \qquad (7)$$

where $\alpha = \alpha_{fy}$ and $\alpha_{fy} = 0.074 - 0.040 f_y/414$ for yield stress; and $\alpha = \alpha_{fu}$ and $\alpha_{fu} = 0.019 - 0.009 f_u/414$ for ultimate stress. Eq. (7) is valid for reinforcement with yield stress between 290–710 MPa and for strain rates between 10^{-4} and 225 s^{-1}.

Erosion Criterion

The simulation is set to display erosion of elements. As such, when the inherent capacity of any element is exceeded during the simulation, it would result in erosion of the element in the model. The principal tensile strain criterion was used to determine the erosion of the elements in this study.

Validation of Finite-Element Models

An explosive loading laboratory testing program conducted at the University of California, San Diego used a hydraulic-based blast simulator to simulate explosive events without using explosive materials Hegemier et al. (2006). Several tests have been performed to investigate the dynamic response of the RC columns when subjected to such impulsive loads.

The dynamic responses of the test specimens subjected to impulse loads of 5.3, 12.1, 13.1, and 15.9 kPa-sec were analyzed using proposed FE models. Three cases of positive duration, representative of typical energy dissipation time of a close-in explosion, were 3, 4, and 5 ms, and their respective peak pressures were used in the analysis, because the detailed peak pressure and duration for the corresponding impulse loads were not reported.

Fig. 4 shows the comparisons of residual deformations of numerical, laboratory, and field test results. The comparisons show that the numerical result is much higher than the laboratory test result when subjected to an impulse load of 12.1 kPa-sec. For the other cases, the comparisons generally show a good agreement. Considering that only limited data were available and the character of blast test results was unstable, these comparisons are considered to be reasonably in good agreement. Good correlations of failure mechanisms are also observed, as shown in Fig. 5. It is apparent from both the field test and blast simulator results that the column failed primarily in diagonal shear near the top and bottom ends, whereas the central portion remained relatively intact. The predicted damage on the column by the FE model is shown by plotting fringes of effective strain, which is used for measuring the overall deformation at one point. These

effective strain contours reveal the strain localization at which failure propagates. The failure is localized near the column top and bottom ends owing to diagonal shear failure, which is consistent with field and laboratory test results. This validates the FE model to be able to predict the residual deflection of RC columns subjected to blast loadings.

Analysis Steps and Load Patterns

The purpose of the validated FE simulation was to obtain the residual deflection of the column specimen at three specific locations at which the actuators were positioned in the laboratory. This deflection would then be programmed into the displacement-controlled actuator settings during the experimental study phase to achieve a column deflection profile to simulate the effect from a blast load. As shown in Fig. 6, the analysis step would begin by applying the service loadings onto the column model. An axial load of $0.4f'_cA_g$ is intended to be applied on specimens S1 and S2, whereas an axial load of $0.2f'_cA_g$ is intended to be applied on specimens S3 and S4. The gravity loading was initially applied in a quasi static method on the steel plate that is on top of the RC column model. Subsequently, dynamic blast pressures were applied to the front face of the column model. The last stage from the numerical modeling program involved determining the residual lateral deflection profile attained by the column model. The target residual deflection of each specimen is shown in Table 1. Moreover, the residual deflections attained by the models are shown in Fig. 7.

Experimental Program

Material Proprieties

Each of the four specimens was cast with ready-mixed concrete that was specified to be able to achieve a characteristic strength of no lower than 25 MPa within 28 days. The aggregates were specified to have a size of 13.0 mm, and the concrete pour was required to produce a slump of 125.0 mm to ensure its workability. Twelve 150 × 300-mm test cylinders (three per individual specimen) were also cast and cured under the same conditions to make them representative of their respective column specimens. The cylinders were individually tested for their compressive strength f'_c to determine the compressive strengths of the concrete used to cast the specimens. The results obtained from the cylinder compressive tests are shown in Table 2. The compressive strengths of the respective specimens were used to carry out the numerical simulations as well.

High tensile strength steel bars of 16.0-mm diameter with nominal yield strength of 460 MPa made up the longitudinal reinforcement, and mild steel bars of 6.0-mm diameter with nominal yield strength of 250 MPa were provided as transverse reinforcement for all column specimens. The two batches of specimens had variations in terms of the amount of transverse reinforcement. The first batch had double hoops formed by R6 bars placed at 100.0-mm spacing. The second batch had single hoops formed by R6 bars placed at 175.0-mm spacing. Table 1 shows the specimen reinforcement specifications.

Test Setup

The experiment setup required a loading frame that was capable of maintaining axial loads on these column specimens initially, subsequently followed by the application of lateral loads to enable the specimens to take up the deflected shape as achieved from the numerical study conducted on the models of these specimens. Once the specimens had achieved the deflected shape as if they had been damaged from a blast load, their axial loads were gradually increased to determine the additional amount of residual axial capacity available on sustaining this simulated blast damage. A sketch and photograph of the test setup

are shown in Fig. 8. The two vertical actuators shown in Fig. 8 worked together with a transfer beam to apply the axial load and measure the residual capacity of the column specimens. Three horizontal actuators were used to deform the column to simulate the effects of blast loadings. Three horizontal rollers were used to constrain the rotation and horizontal freedom of the top head.

Instrumentation

Extensive measuring devices were used to monitor the response of the test specimens on the specimens and within the actuators. The built-in load cells in the actuators were used to measure the axial load and residual axial capacity of the specimens. Three LVDTs capable of a travel distance of 300 mm were used to monitor the horizontal deflection of the column.

Experimental Results and Observations

Specimen S1

A target midheight deflection of 27.8 mm, or a midheight deflection ratio (MHDR) (defined as the ratio of the midheight deflection to the height of the column) of 1.16%, was to be attained on this specimen. The axial load of 811 kN ($0.4f'_cA_g$) was applied through a displacement-controlled mode through the vertically placed actuators. Once the preaxial load was maintained, the lateral actuators were controlled through a displacement-controlled mode to achieve the targeted displacement profile of this specimen. The crack development pattern that was observed during the experiment is shown in Fig. 9(a). As shown in Fig. 9(a), the flexural cracks were observed in the midheight of the column at an MHDR of 0.2%. The first diagonal shear crack occurred in the bottom end of the column when the MHDR reached 0.5%. The diagonal shear cracks at the bottom of the column became wider, and the midheight flexural cracks developed toward the top end of the column when the MHDR was further increased to 1.0%. As the MHDR neared the targeted value of 1.18%, diagonal shear cracks were also observed at the top of the column. Photographs of specimen S1 being subjected to the lateral loads are shown in Fig. 10. A plot of the experimental deflected profile of specimen S1 and the other specimens are shown in Fig. 11.

Fig. 12(a) shows the applied axial loads against the respective vertical deformations of specimen S1. The initial axial load of 811 kN, as shown in Fig. 12(a), caused a vertical shortening of column specimen S1 by approximately 4 mm. The lateral loads were then applied to the column specimen. This increased the vertical shortening to approximately 6.7 mm. In the final axial loading phase, the laterally damaged column specimen was able to sustain a further axial loading of approximately 982 kN before it took a dip. The test was brought to a halt when the axial load that the column specimen could carry dropped to 424 kN. The column specimen had shortened by approximately 16.0 mm at that axial load.

Specimen S2

The numerically predicted target lateral deflection for S2 was 46.8 mm, or an MHDR of 1.95%, and the axial load was similar to that of S1 at 811 kN ($0.4\ f'_cA_g$). The first flexural cracks were observed in the midheight of the column at a, MHDR of 0.17%, and the cracks were seen to develop toward the top of the column rapidly. The first signs of diagonal shear cracks forming were observed in the bottom end of the column at an MHDR of 0.75%. At this MHDR, the flexural cracks in the top end of the column become slightly oblique. When S2 attained an MHDR of 1.67%, wide diagonal shear cracks were formed in both ends of the column, and slight concrete compressive crushing occurred in the column. A plot of the applied axial loads against the respective vertical deformations of column specimen S2 is shown in Fig. 12(b). Fig. 12(b) shows that the initial axial load of 811 kN caused a vertical shortening of column S2 of approximately

5.9 mm. The lateral loads were then applied to the column specimen. When the lateral actuators were almost about to achieve the targeted deflection profile of this specimen, a sudden drop of the axial load that the column was sustaining occurred. This plummet in the axial load occurred at a vertical displacement of approximately 9.0 mm. The axial load at this point dropped to approximately 680 kN. Subsequently, the lateral loading was stopped, and the specimen was put through further axial load increments to determine if it possessed any residual axial capacity. The axial loading at this point rose to a peak value of approximately 771 kN and then failed to rise any further from that point. The experiment was brought to a halt when the axial load dropped further to 380 kN, and the column specimen had shortened by almost 11.0 mm.

Specimen S3

The targeted midheight deflection to be achieved on this specimen was 53.4 mm, or an MHDR of 2.22%, and the specimen was axially loaded to 406 kN ($0.2f'_cA_g$). The crack development pattern that was observed during the experiment is shown in Fig. 9(c). In general, the crack development pattern of specimen S3 was similar to that of S2. Initially, the first crack occurred in the midheight region at an MHDR of 0.25% and then developed toward both ends of the column. The first signs of diagonal shear cracks forming were observed in the bottom of the column at n MHDR of 0.83%. The diagonal shear cracks at the bottom of specimen S3 grew wider as the MHDR increased, and flexural cracks were seen developing at the top of the column at this stage. As the MHDR closed in toward the numerically predicted target, diagonal shear cracks were formed on both ends of S3. Fig. 12(c) shows the applied axial loads plot against the respective vertical deformation of specimen S3. Fig. 12(c) that the initial axial load of 406 kN on specimen S3 caused a vertical shortening of approximately 3.0 mm. The application of the lateral loads subsequently increased the vertical shortening to approximately 9.0 mm. In the final axial loading phase, the laterally damaged column specimen was able to sustain a further axial loading of approximately 535 kN before its load-bearing capacity started to take a dip. The test was brought to a halt when the axial load that the column specimen could carry dropped to 190 kN. Specimen S3 had shortened by approximately 14.0 mm at that axial load.

Specimen S4

Specimen S4 was also under an axial load of 406 kN ($0.2\ f'_cA_g$), similar to that of S3. The numerically predicted target midheight lateral displacement was approximately 65 mm, or an MHDR of 2.74%. The crack development pattern of specimen S4 that was observed during the experiment is shown in Fig. 9(d). Flexural cracks were observed in the midheight of the column, as shown in Fig. 9(d) at an MHDR of 0.33%. Severe flexural cracking was seen to develop toward both ends of the columns as the MHDR increased. Diagonal shear cracks were observed in both ends of the column as the MHDR reached toward 1.75%. Slight concrete spalling was also observed in the bottom of the column at this stage. As the MHDR reached toward the numerically predicted target value, a significant amount of concrete loss occurred at the top and bottom of specimen S4 owing to axial compression and shear. As shown in the Fig. 12(d), the axial load of 406 kN caused a vertical shortening of specimen S4 by approximately 3.6 mm. The lateral loads applied to specimen S4 further increased the vertical shortening to approximately 10.5 mm. In the final axial loading phase, the laterally damaged column specimen was able to sustain an additional axial loading of approximately 526 kN before it started to dip. The test was brought to a halt when the axial load that the column specimen could carry dropped to 280 kN. The column specimen had shortened by approximately 13.5 mm at that axial load.

Discussion of Experimental Results Lateral Displacements

Lateral Displacements

Fig. 11 shows the deflected profile of all four numerical models and experimental specimens. Both numerical and experimental results indicated that the LS series of specimens with a higher transverse reinforcement ratio have a less extreme lateral deflection profile. Moreover, the reduced axial load in specimens S2 and S4 resulted in the column being less stiff globally. This reduced global stiffness of the column produced a comparatively more extreme deflected profile in those specimens. Table 3 shows the lateral displacements at specific heights of the four models and specimens. It can be observed that the deflection profile reproduced by the static hydraulic actuators was not an exact match when compared with the numerically predicted blast-damaged profiles. However, the maximum displacement in the midheight of the column specimens were controlled during the experiment to achieve midheight deflections that were as close as possible to each of their numerical counterparts.

Residual Axial Capacities

Fig. 12 shows the experimental axial load history of each specimen. As shown in Fig. 12, all of the specimens except specimen S2 had sufficient axial capacity to sustain its axial loading despite attaining its respective laterally deflected form. The lower transverse reinforcement ratio within the S2 caused it to have a lower shear resistance compared to with specimen S1, which was also loaded with the same axial load. The poor shear resistance in turn caused the column to have a severe deflected profile when damaged by the same blast wave that was imposed on all specimens. In contrast, specimen S4, with the same amount of transverse reinforcement as specimen S2, was able to sustain its axial load despite being displaced to an MHDR of almost 2.6%.

Verifying Prediction Equation

An equation that was capable of predicting the blast-damaged residual axial capacity of RC columns was proposed by Bao and Li (2010). The prediction considered parameters such as longitudinal and transverse reinforcement ratios, column aspect ratio, residual midcolumn deflection, and applied axial loading. A bar chart showing the respective residual axial capacities of the experimental specimens and their respective predicted residual axial capacities is shown in Fig. 13. It is evident from the bar chart in Fig. 13 that when the equation was used to predict the residual axial capacities of specimens S1 and S3, it resulted in large overestimates. This is because the form of the equation cannot analyze column specimens with higher transverse reinforcement ratio. It was also observed from the study that for columns with higher transverse reinforcement ratios, the equation provided a residual axial capacity prediction that was greater as the blast-damaged residual midcolumn deflection increased. However, for the specimens with lower transverse reinforcement ratio, this was not the case. The equation was able to predict the residual axial capacity of specimens S2 and S4 with an accuracy of approximately 20%. The residual axial capacities of all four of specimens are shown in Table 4.

Conclusions

The following conclusions can be drawn on the basis of the experimental and numerical study results:

The results obtained indicate that an axial loading of 0. $f'_c A_g$ that was applied on specimens S1 and S2 before the lateral loadings resulted in those specimens having a less extreme lateral deflection profile compared with S3 and S4. It can be concluded that higher axial loading caused increased stiffness, which resulted in a smaller deflected profile. This is because increasing axial load increases the moment capacity and nominal shear strength of RC columns.

However, if the impulse and the corresponding displacement exceed certain critical values, the lateral displacement would increase tremendously with increasing axial load owing to the P - δ effect. This effect is

more prominent in columns with lower transverse reinforcement ratios.

The LS series of specimens (S1 and S3) with higher transverse reinforcement ratios provided additional shear strength. This additional shear strength resulted in these models and specimens attaining a smaller lateral residual deflection profile compared with the NS series of specimens (S2 and S4). The NS detailing, usually used in low seismicity regions, is primarily designed with no special consideration for ductility demand. This usually causes the column to fail through a diagonal shear mode. The LS detailing provides additional restraint for the longitudinal bars and provides increased confinement for the core concrete. This improves the shear capacity of the column. The numerical results from all of the models show that the increase in transverse reinforcement ratio significantly reduced the degree of direct blast-induced damage on the columns.

The results obtained from specimens S1 and S3 show that both these columns had sufficient residual axial capacity to sustain their prescribed axial loads. The increased transverse reinforcement in these models and specimens reduced the severity of the lateral displacement profile they attained owing to the lateral loads. This less severe damaged state in turn provided them with a higher residual axial capacity.

The NS detailed specimen S2 has a more severe lateral deflection profile compared with the LS detailed specimen S1. This damage profile resulted in these models and specimens being unable to sustain the prescribed axial load. In contrast, specimen S4 had a laterally deflected profile even more severe than that attained by specimen S2. This was owing to the lower axial load that was prescribed on specimen S1. However, despite the more severe lateral deflected profile attained by specimen S4, this column had sufficient capacity to sustain its axial loading.

On verifying the blast-damaged residual axial capacity of the RC column equation that was proposed by a previously conducted parametric study, some flaws surfaced. The equation is able to predict with decent accuracy for columns with low transverse reinforcement. However, it provides a rather large overestimate of the residual axial capacity for columns with higher transverse reinforcement ratios. The applicability of this equation must be improved through future studies.

Acknowledgments

This research was supported by a research grant provided by the Defense Science and Technology Agency (DSTA), Singapore, under the Protective Technology Research Center, Nanyang Technological University, Singapore. Any opinions, findings, and conclusions expressed in this paper are those of the writers and do not necessarily reflect the view of DSTA, Singapore.

Notation

The following symbols are used in this paper:

A_g = gross area of the section;
C = rank 4 stiffness tensor of the material;
E = internal energy per initial volume;
f_c = compressive strength of concrete;
$f'c$ = characteristic cylinder compressive strengths of the concrete;
f_u = ultimate strength of reinforcement;
f_y = static yield strength of reinforcement;
L = clear height of column;
P_L = long-term axial load;
P_{max} = axial capacity of the undamaged column;
P_r = residual axial capacity of a blast-damaged column;
p = pressure;
r_f = strain rate enhancement factor;
T = hydrostatic tension cut off to the point T of elastic limit;
v = ratio of residual axial capacity;
y_r = residual mid height displacement;
ρ_g = longitudinal reinforcement ratio;
ρ_v = volumetric ratio of transverse reinforcement;
σ = cauchy stress tensor;
$\dot{\varepsilon}$ = strain rate;
$\dot{\varepsilon}_s$ = static strain rate; and
ε_v = volumetric strain.

References

Bao, X., and Li, B. (2010). "Residual strength of blast damaged reinforced concrete columns." *Int. J. Impact Eng.*, 37(3), 295–308.

Crawford, J. E., Malvar, L. J., Morill, K. B., and Ferritto, J. M. (2001). "Composite retrofits to increase the blast resistance of reinforced concrete buildings." *Proc., 10th Int. Symp. on Interaction of the Effects of Munitions with Structures*, Structural Engineer, San Diego, 1–13.

Hallquist, J. Q. (2008). LS-DYNA *user's keyword manual, version 971, Livermore* Software Technology Corporation, Livermore, CA.

Hayes, J. R. Jr., Woodson, S. C., Pekelnicky, R. G., Poland, C. D., Corley, W. G., and Sozen, M. (2005). "Can strengthening for earthquake improve blast and progressive collapse resistance." *J. Struct. Eng.*, 131(8), 1157–1177.

Hegemier, G. A., Seible, F., Rodriguez, N. T., and Arnett, K. (2006). "Blast mitigation of critical infrastructure components and systems." *Proc., 2nd FIB Int. Congress*, Naples, Italy.

Krauthammer, T., Hall, R. L., Woodsoon, S. C., Baylot, J. T., Hayes, J. R., and Sohn, Y. (2003). "Development of progressive collapse analysis procedure and condition assessment for structures." *Proc., National Workshop on Prevention of Progressive Collapse in Rosemont*, National Institute of Building Sciences, Washington, DC.

Li, B., Pan, T. C., and Nair, A. (2009). "A case study of the effect of cladding panels on the response of reinforced concrete frames subjected to distant blast loadings." *Nucl. Eng. Des.*, 239(3), 455–469.

Li, B., Pan, T. C., and Nair, A. (2011). "A case study of the local and global structural responses of a tall building in singapore subjected to close-in detonations." *Struct. Des. Tall Special Build.*, 20(2), 223–246.

Malvar, L. J., and Crawford, J. E. (1998). "Dynamic increase factors for steel reinforcing bars." *Proc., 28th Department of Defense Explosives Safety Board (DDESB) Seminar*, Orlando, FL, 1–17.

Malvar, L. J., Crawford, J. E., Wesevich, J. W., and Simons, D. (1997). "A plasticity concrete material model for DYNA3D." *Int. J. Impact Eng.*, 19(9–10), 847–873.

Randers-Pehrson, G., and Bannister, K. A. (1997). "Air blast loading model for DYNA2D and DYNA3D." *Rep. ARL-TR-1310*, Army Research Laboratory, Adelphi, MD.

Schwer, L. E., and Malvar, L. J. (2005). *Simplified concrete modeling with *mat_concrete_damage_rel3*, Japan Research Institute, Ngoya, Japan.

Wu, K.-C., Li, B., and Tsai, K. C. (2011). "Residual axial compression capacity of localised blast damaged RC columns." *Int. J. Impact Eng.*, 38(1), 29–40.

List of tables

List of figures

Test	Height (mm)	Cross-section (mm × mm)	Longitudinal rebar (%)	Transverse reinforcement (%)	Axial load (kN)	$X^{FEM}_{midheight}$ (mm)	MHDR (%)
S1	2,400	260 × 260	2.30	0.58	810	28.3	1.18
S2	2,400	260 × 260	2.30	0.19	810	41.2	1.94
S3	2,400	260 × 260	2.30	0.58	406	52.8	2.20
S4	2,400	260 × 260	2.30	0.19	406	64.8	2.69

Note: MHDR = the ratio of the midheight deflection to the height of the column; $X^{FEM}_{midheight}$ = predicted residual deflection in the midheight of the column.

Table 1

Test	Cylinder 1 f'_c (MPa)	Cylinder 2 f'_c (MPa)	Cylinder 3 f'_c (MPa)	Average f'_c (MPa)
S1	27.8	34.8	32.7	31.8
S2	35.3	30.9	31.8	32.6
S3	32.6	32.7	34.7	33.3
S4	30.3	34.8	32.5	32.6

Table 2

Test	Finite-element model node height (mm)	Predicted lateral displacement (mm)	Lateral actuator height (mm)	Experimental lateral displacement (mm)
S1	600	18.19	530	28.92
	1,200	27.77	1,200	30.14
	1,800	22.18	1,870	24.96
S2	600	36.78	530	44.68
	1,200	46.81	1,200	41.23
	1,800	36.83	1,870	34.96
S3	600	33.15	530	38.50
	1,200	53.38	1,200	55.03
	1,800	36.49	1,870	51.91
S4	600	44.05	530	61.70
	1,200	65.94	1,200	61.17
	1,800	43.77	1,870	49.05

Table 3

Table 4. Residual Axial Capacities of Models and Specimens

Residual axial capacity	S1	S2	S3	S4
Experimental (kN)	982	771	535	526
Equation (kN)	1,520	842	1,342	473

Table 4

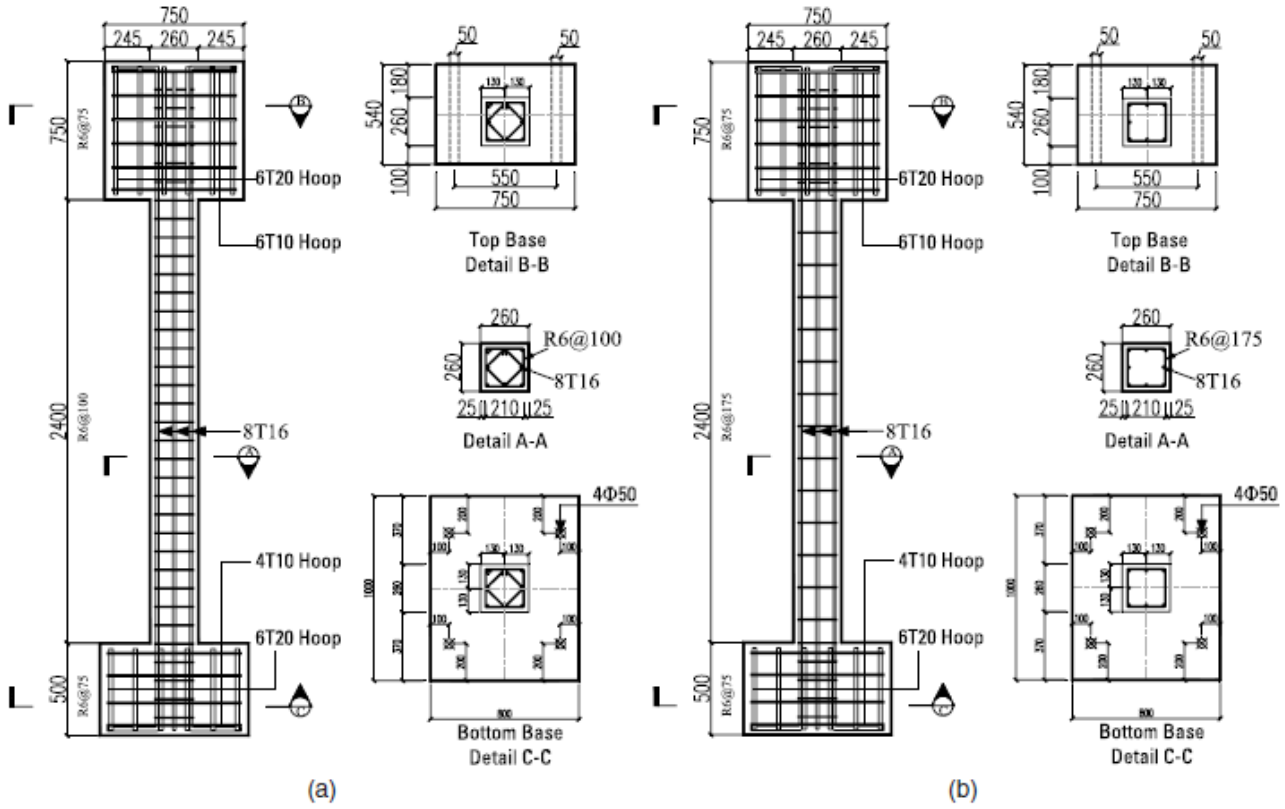
750
245 260 245
750
R6@75
6T20 Hoop
6T10 Hoop
2400
R6@100
8T16
4T10 Hoop
6T20 Hoop
500
R6@75
50
50
540
260
180
100
550
750
Top Base
Detail B-B
260
260
R6@100
8T16
25 210 25
Detail A-A
4Φ50
1000
800
Bottom Base
Detail C-C
(a)
750
245 260 245
750
R6@75
6T20 Hoop
6T10 Hoop
2400
R6@175
8T16
4T10 Hoop
6T20 Hoop
500
R6@75
50
50
540
260
180
100
550
750
Top Base
Detail B-B
260
260
R6@175
8T16
25 210 25
Detail A-A
4Φ50
1000
800
Bottom Base
Detail C-C
(b)

Figure 1

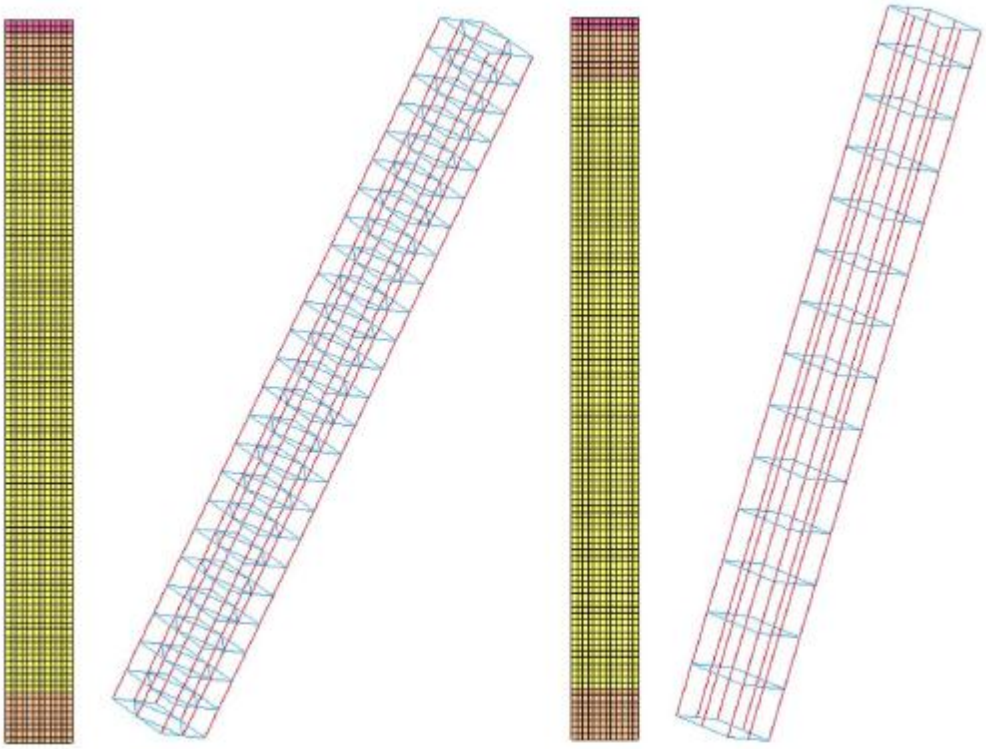

Figure 2

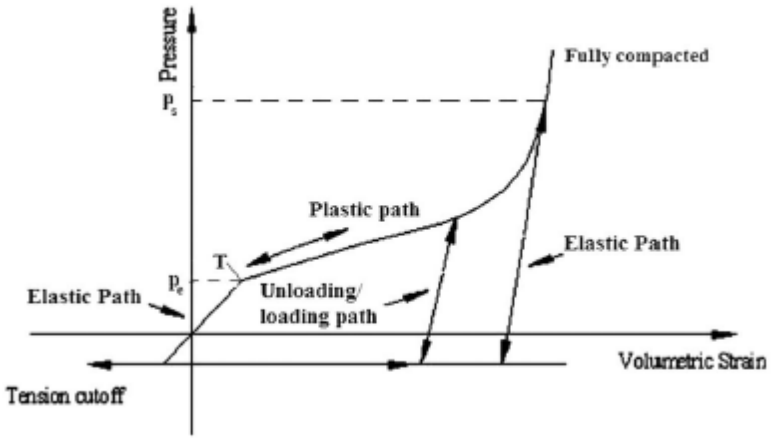
Pressure
p_s
Fully compacted
Plastic path
Elastic Path
T
p_e
Elastic Path
Unloading/
loading path
Volumetric Strain
Tension cutoff

Figure 3

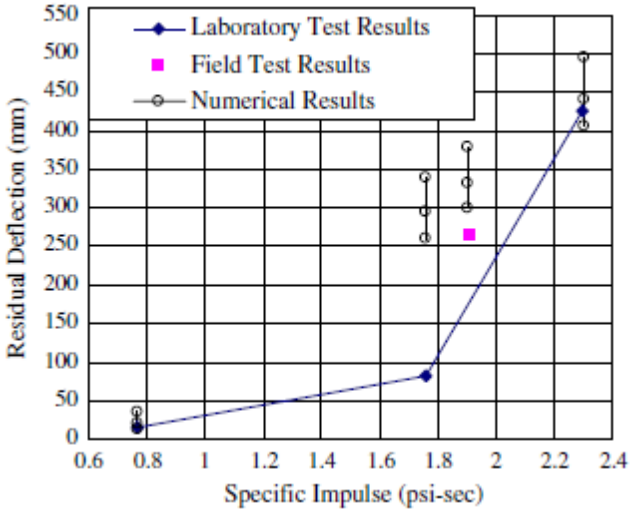
Laboratory Test Results
Field Test Results
Numerical Results
Residual Deflection (mm)
550
500
450
400
350
300
250
200
150
100
50
0
0.6
0.8
1
1.2
1.4
1.6
1.8
2
2.2
2.4
Specific Impulse (psi-sec)

Figure 4

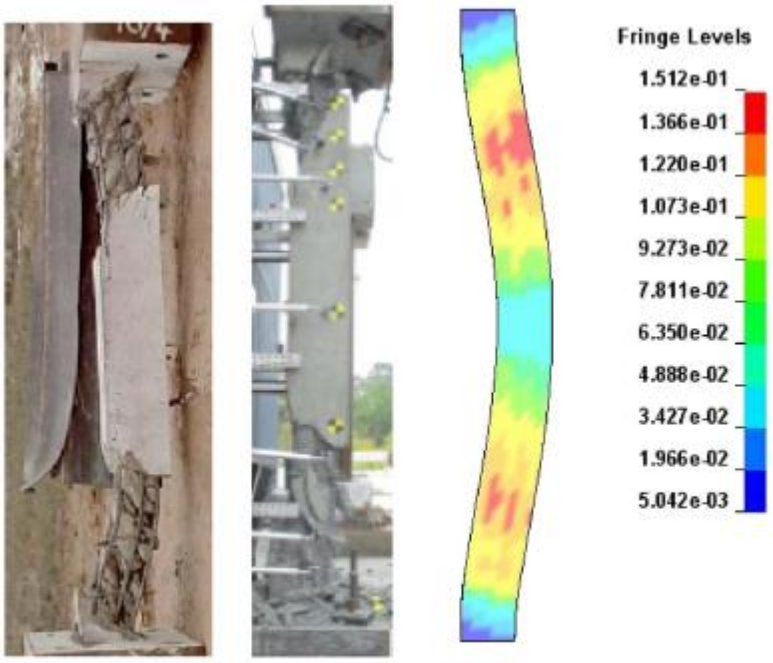
Fringe Levels
1.512e-01
1.366e-01
1.220e-01
1.073e-01
9.273e-02
7.811e-02
6.350e-02
4.888e-02
3.427e-02
1.966e-02
5.042e-03
Field Test
Blast Simulator Test
Predicted Damage

Figure 5

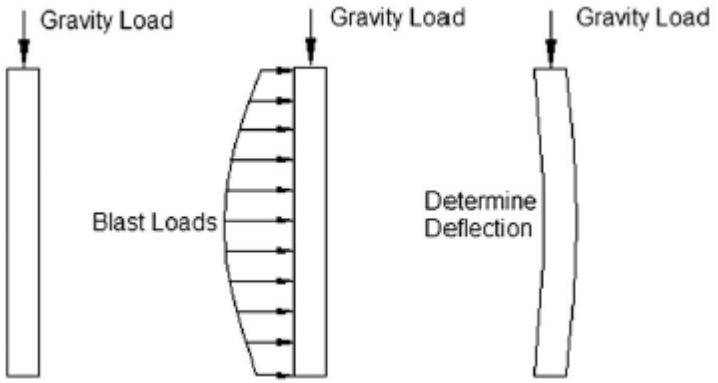
Gravity Load
Gravity Load
Gravity Load
Blast Loads
Determine
Deflection

Figure 6

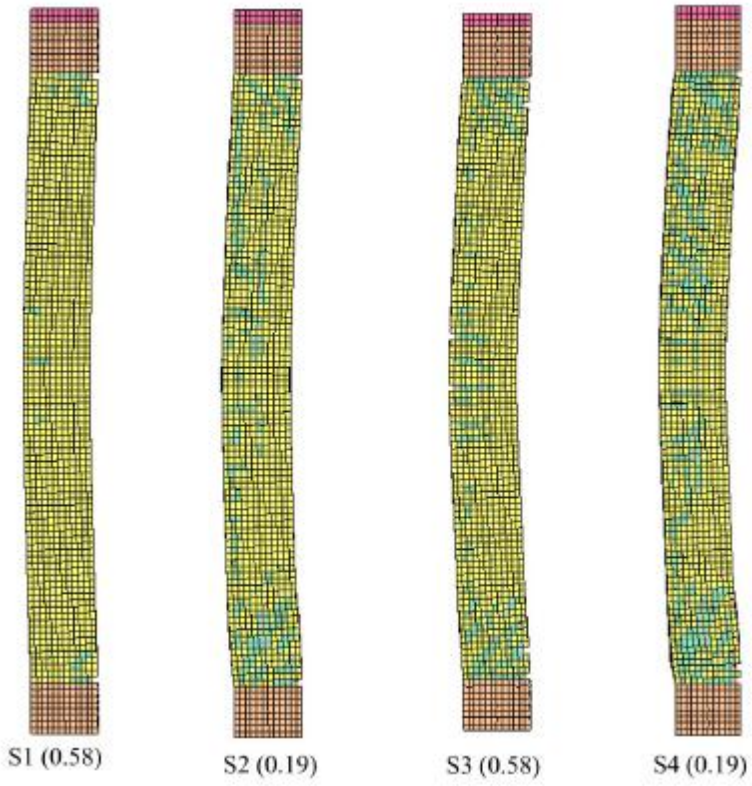

Figure 7

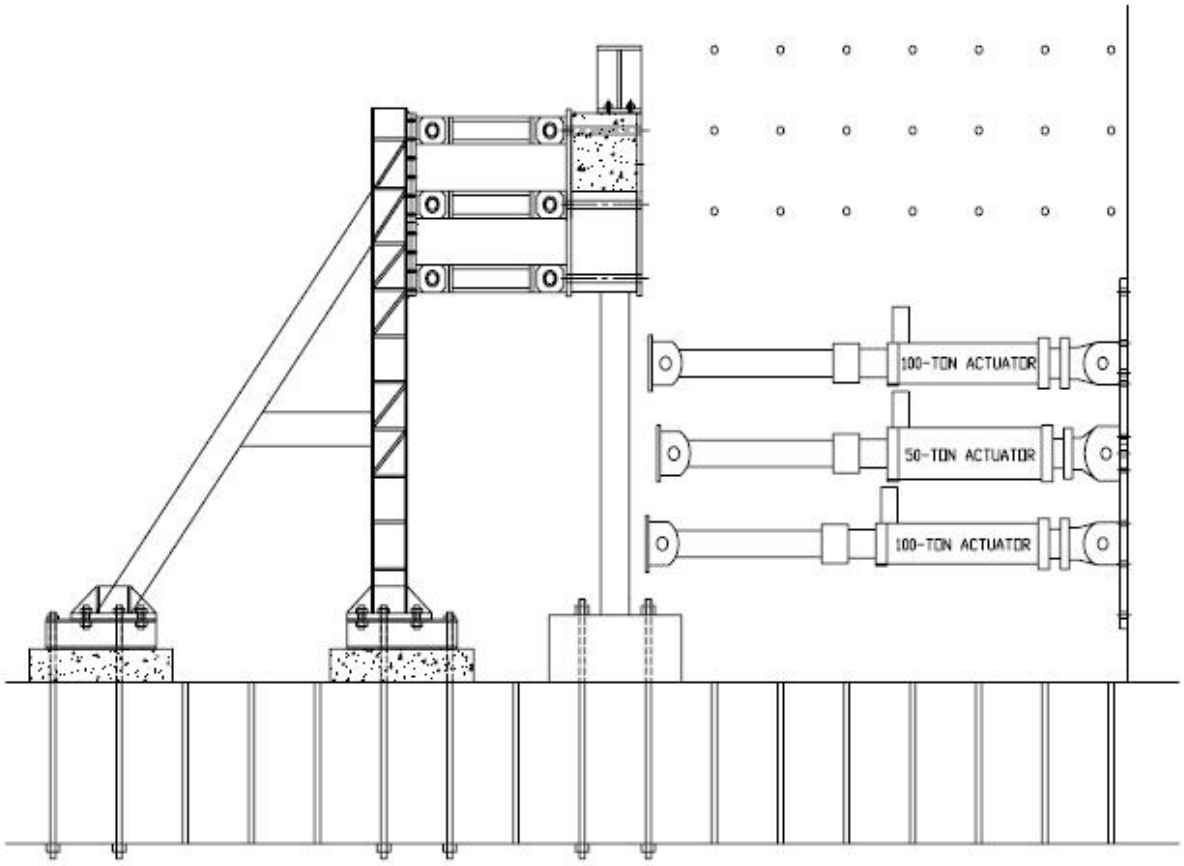

Figure 8

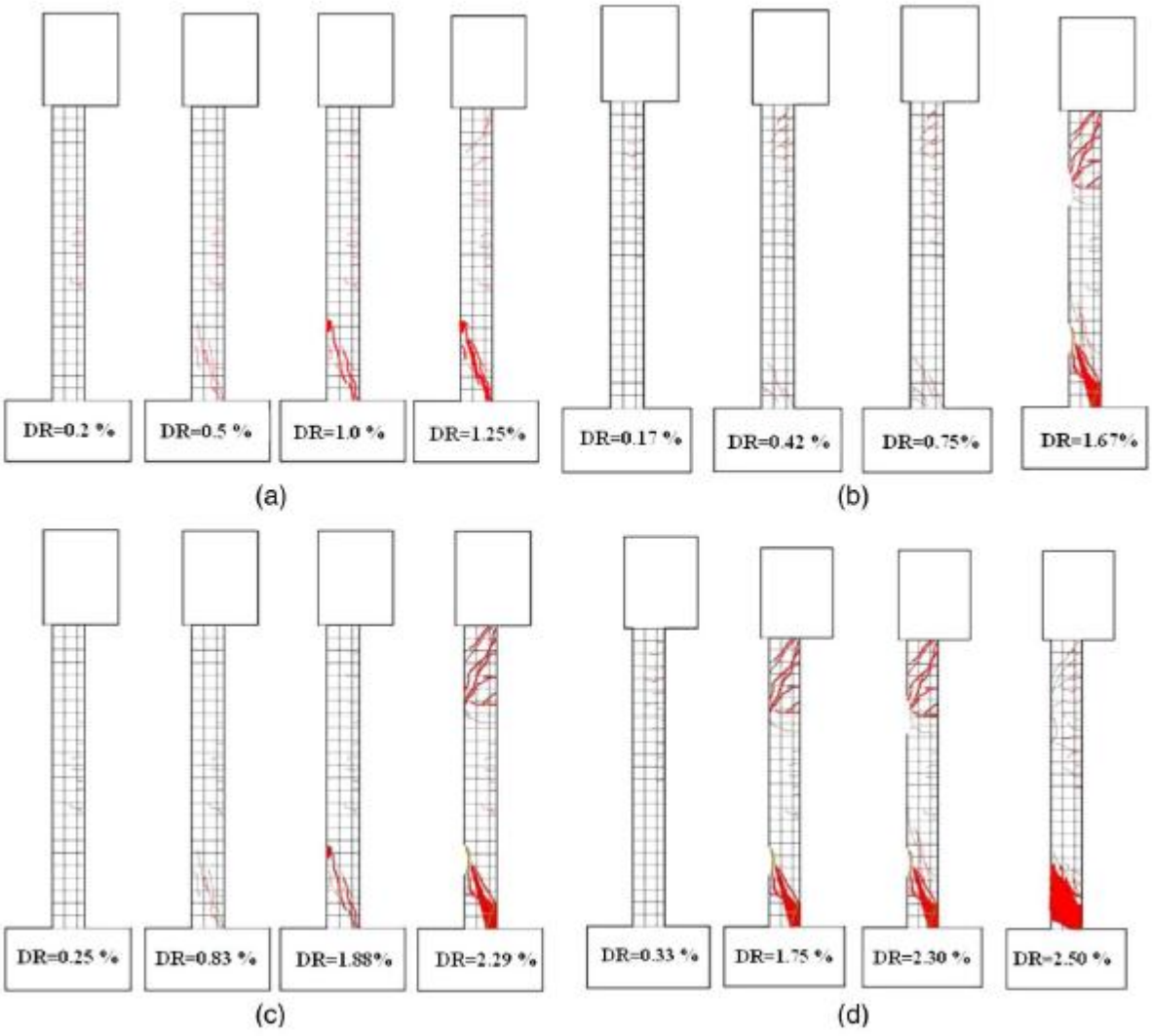
DR=0.2 %
DR=0.5 %
DR=1.0 %
DR=1.25%
(a)
DR=0.17 %
DR=0.42 %
DR=0.75%
DR=1.67%
(b)
DR=0.25 %
DR=0.83 %
DR=1.88%
DR=2.29 %
(c)
DR=0.33 %
DR=1.75 %
DR=2.30 %
DR=2.50 %
(d)

Figure 9

Figure 10

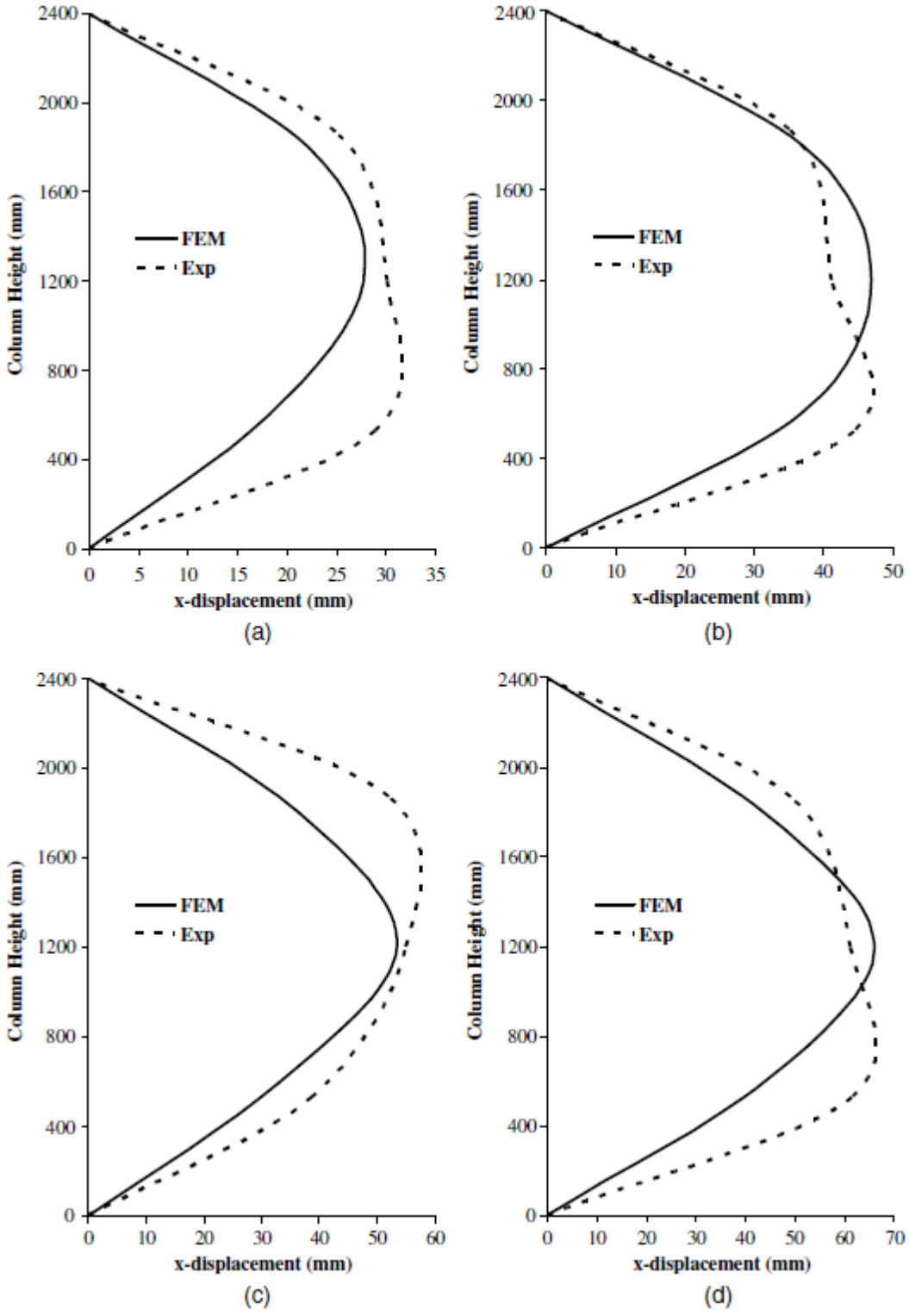

Figure 11

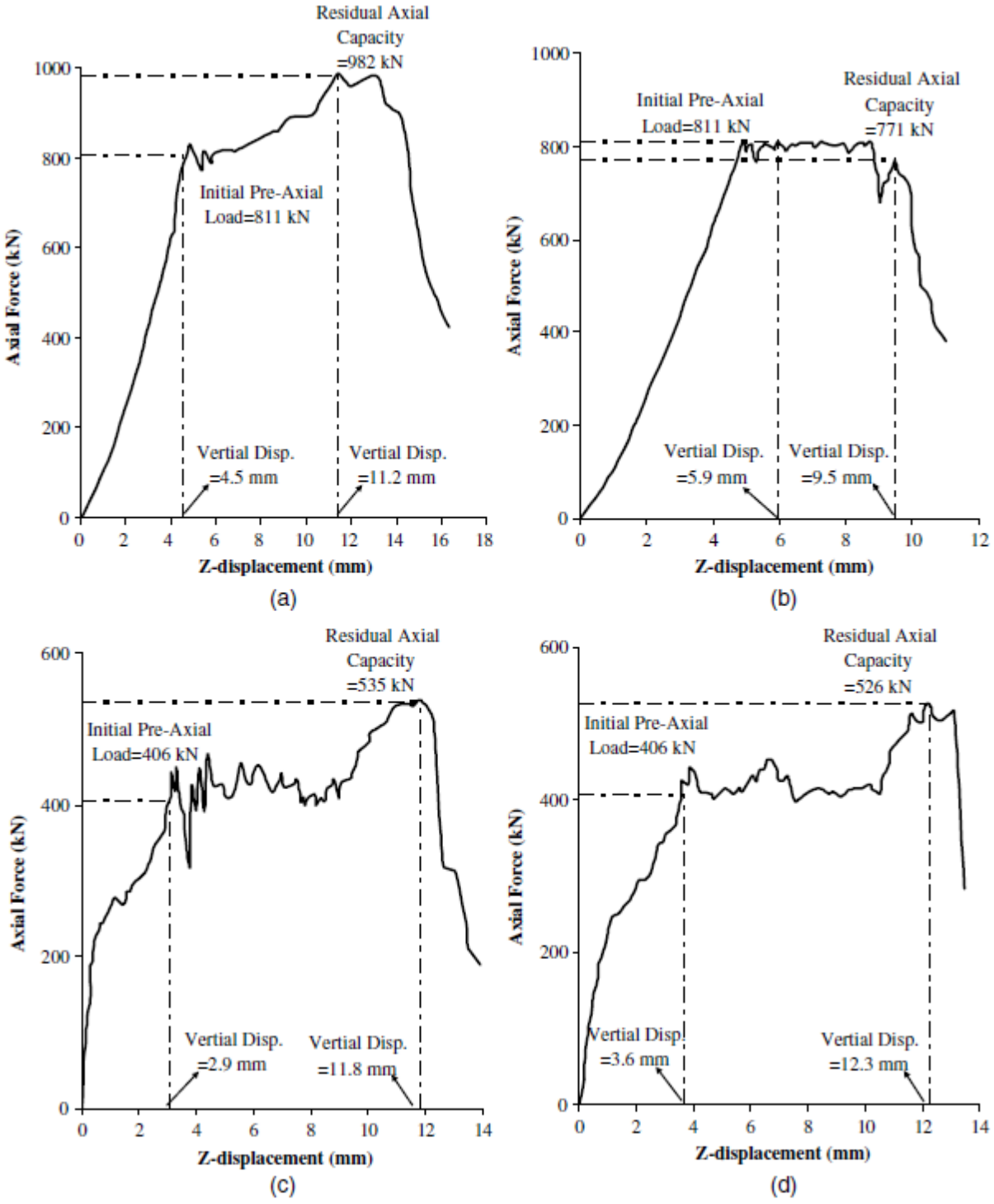
Residual Axial Capacity =982 kN
Initial Pre-Axial Load=811 kN
Vertial Disp. =4.5 mm
Vertial Disp. =11.2 mm
Axial Force (kN)
Z-displacement (mm)
(a)
Initial Pre-Axial Load=811 kN
Residual Axial Capacity =771 kN
Vertial Disp. =5.9 mm
Vertial Disp. =9.5 mm
Axial Force (kN)
Z-displacement (mm)
(b)
Residual Axial Capacity =535 kN
Initial Pre-Axial Load=406 kN
Vertial Disp. =2.9 mm
Vertial Disp. =11.8 mm
Axial Force (kN)
Z-displacement (mm)
(c)
Residual Axial Capacity =526 kN
Initial Pre-Axial Load=406 kN
Vertial Disp. =3.6 mm
Vertial Disp. =12.3 mm
Axial Force (kN)
Z-displacement (mm)
(d)

Figure 12

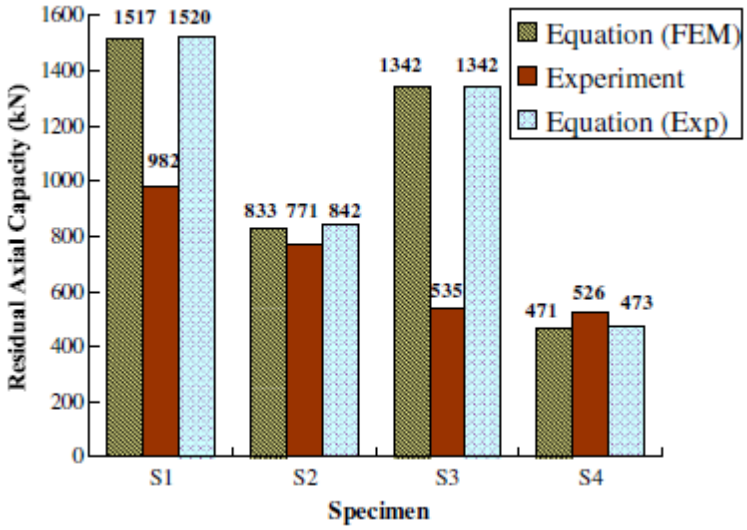
Residual Axial Capacity (kN)
1600
1400
1200
1000
800
600
400
200
0
1517
1520
982
833
771
842
1342
1342
535
471
526
473
S1
S2
S3
S4
Specimen
Equation (FEM)
Experiment
Equation (Exp)

Figure 13